

pubs.acs.org/NanoLett Letter

Atomic Layer Deposition of Cu Electrocatalysts on Gas Diffusion Electrodes for CO₂ Reduction

Julia D. Lenef, Si Young Lee, Kalyn M. Fuelling, Kevin E. Rivera Cruz, Aditya Prajapati, Daniel O. Delgado Cornejo, Tae H. Cho, Kai Sun, Eugenio Alvarado, Timothy S. Arthur, Charles A. Roberts,* Christopher Hahn, Charles C. L. McCrory, and Neil P. Dasgupta*



Cite This: Nano Lett. 2023, 23, 10779-10787



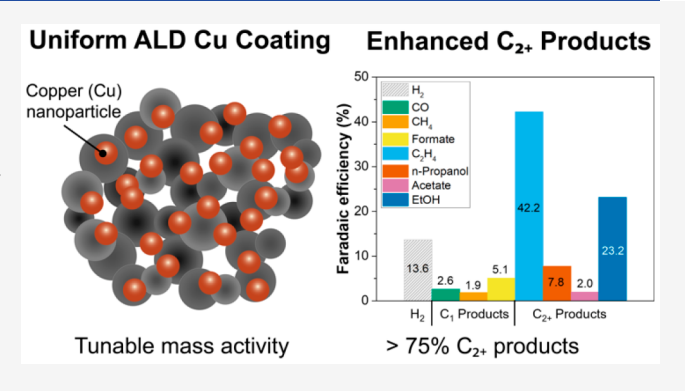
ACCESS I

Metrics & More

Article Recommendations

Supporting Information

ABSTRACT: Electrochemical reduction of CO_2 using Cu catalysts enables the synthesis of C_{2+} products including C_2H_4 and C_2H_5OH . In this study, Cu catalysts were fabricated using plasma-enhanced atomic layer deposition (PEALD), achieving conformal deposition of catalysts throughout 3-D gas diffusion electrode (GDE) substrates while maintaining tunable control of Cu nanoparticle size and areal loading. The electrochemical CO_2 reduction at the Cu surface yielded a total Faradaic efficiency (FE) > 75% for C_{2+} products. Parasitic hydrogen evolution was minimized to a FE of ~10%, and a selectivity of 42.2% FE for C_2H_4 was demonstrated. Compared to a line-of-sight physical vapor deposition method, PEALD Cu catalysts show significant suppression of C_1 products compared to C_{2+} , which is associated



with improved control of catalyst morphology and conformality within the porous GDE substrate. Finally, PEALD Cu catalysts demonstrated a stable performance for 15 h with minimal reduction in the C_2H_4 production rate.

KEYWORDS: atomic layer deposition, CO₂ reduction, gas diffusion electrode, copper, catalyst

To address the growing challenges surrounding climate change, there is significant interest in using the electrochemical reduction of CO_2 (CO_2RR) to form value-added products. Copper has been identified as the only single-element catalyst to form a wide range of multicarbon products such as C_2H_4 and C_2H_5OH . Although at least 16 unique products have been identified, the product selectivity varies significantly with the applied potential, catalyst composition, cell design, and electrolyte composition. Sp. By modification of these parameters, the local pH, surface binding energy, active sites, and surface defects can be engineered to alter the product distribution.

For example, by systematically engineering Cu mesopores of various sizes, the local pH can be modified, where smaller pores have been shown to increase the Faradaic efficiency (FE) of C₂ products by increasing the retention times for reaction intermediates.⁷ The reaction intermediates can also be altered by alloying Cu with transition metals such as Ag and Zn, shift has been found to improve the C₂₊ product selectivity. The catalyst layer thickness, deposition method, and nanoparticle sizes are additional factors that can influence product selectivity. Finally, integration of Cu-based catalysts onto 3D gas diffusion electrodes (GDEs) has been shown to further increase performance/current densities toward industrially relevant electrolyzers. Therefore, the future of the

CO₂RR is moving toward complex 3-D structures, where it is important to control the properties of the catalyst throughout the electrode architecture to optimize catalyst utilization and maintain high activity and selectivity.

Currently, most catalyst deposition methods rely on electrodeposition, ¹⁵ spray coating, ¹⁶ solution coating, ^{17,18} or physical vapor deposition (e.g., sputtering/evaporation). ^{16,19,20} However, these methods are often limited by trade-offs between conformality, control of catalyst loading, and the ability to maintain tunable control of particle size at the nanoscale, especially when adding catalysts to 3D supports such as GDEs. In particular, line-of-sight methods may introduce large gradients in the catalyst loading onto high-aspect-ratio substrates such as GDEs. ²¹ As a result of local variations in the surface chemistry, morphology, and mass activity, conventional deposition methods can therefore result

Received: August 2, 2023 Revised: November 16, 2023 Accepted: November 16, 2023

Published: November 21, 2023





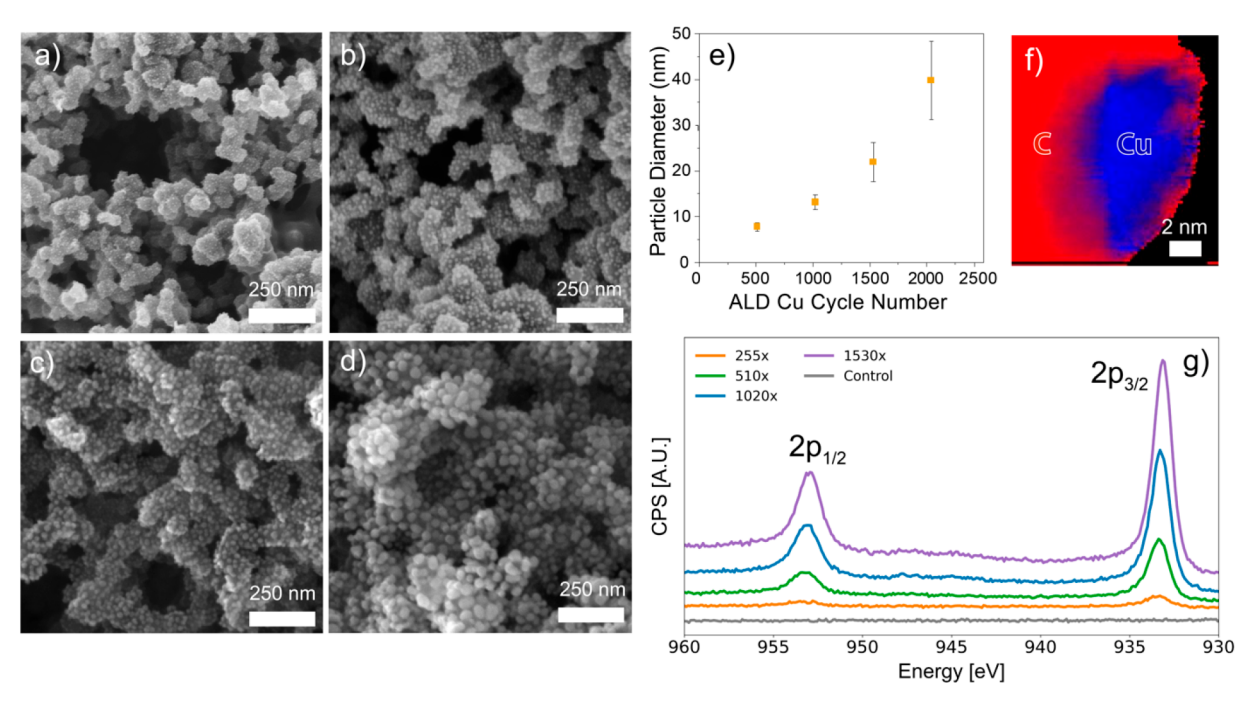


Figure 1. SEM images of PEALD Cu on 3-D GDEs with varied Cu cycle numbers: (a) 510×, (b) 1020×, (c) 1530×, and (d) 2040×. (e) Quantification of particle diameter vs ALD cycle number for the SEM images in (a–d). Error bars represent the standard deviations of 50 unique measurements. (f) EELS map for Cu and C: identical 1020× sample. (g) XPS analysis of PEALD Cu with varied cycle numbers. One minute Ar⁺ sputtering was applied to remove adventitious species.

in a modification of the selectivity, activity, and stability. 14,22-24

To address these limitations, atomic layer deposition (ALD) is a powerful gas-phase deposition technique based on the sequential exposure of a substrate to self-limiting precursor exposures. ALD enables conformal deposition of either continuous films or discrete nanoparticles on high-aspectratio substrates, while maintaining subnanometer precision in composition and loading.²⁵⁻²⁷ For example, recent work demonstrated conformal deposition into porous aerogels with aspect ratios >60000:1.26 As a subvariant of thermal ALD, plasma-enhanced ALD (PEALD) involves the use of a reactive plasma (e.g., H₂, O₂, etc.) as one of the coreactants. The increased kinetic energy and reactivity of the plasma radicals can enable a wider range of processing conditions and improved control of nucleation behavior in metal ALD processes such as Cu, 28-30 which often initiate as discrete nanoparticle islands during the initial ALD cycles.^{31,32}

Owing to these beneficial properties, ALD has enabled the rational design of 3-D catalyst and electrode architectures for a range of reactions, where atomically precise control of catalyst size, surface chemistry, and catalyst—support interactions has been demonstrated.^{33–43} However, although ALD of ZnO and SnO₂ has been previously applied on Cu nanowires to form CuZn⁴⁴ and SnO₂/Cu alloys,⁴⁵ respectively, to date, there has only been one report of ALD of Cu-based electrocatalysts for CO₂RR, which focused on CuS_x and did not report C₂₊ product formation.⁴⁶ Previous efforts have also incorporated low loadings of ALD Cu on TiO₂ for photocatalytic reduction of CO₂ but did not explore electrocatalysis.^{47,48} Therefore, there is strong motivation to explore the ability of ALD processes to systematically tune 3-D electrocatalyst architectures for CO₂RR.

In this work, Cu catalysts were deposited by PEALD onto porous carbon GDEs. This enables tunable catalyst size and loading while maintaining a conformal coating deep into the 3-D electrode surface, without clogging the surface pores. Under optimized conditions, a total C_{2+} product selectivity of 75.2% was measured, with a C_2H_4 selectivity of >42%. Compared with Cu catalysts deposited onto GDEs using physical vapor deposition (PVD), the C_{2+}/C_1 product selectivity is significantly increased when using PEALD, which demonstrates the importance of controlling process—structure relationships to tune the 3-D catalyst architecture. Finally, stable activity was observed for over 15 h using PEALD Cu catalysts.

Figure 1a-d shows a series of scanning electron microscopy (SEM) images of the microporous layers of GDE substrates after they were coated with various numbers of ALD cycles. Because PEALD growth of metallic Cu tends to nucleate as nanoparticle islands, 49 by varying the number of deposition cycles, the Cu particle diameter and areal catalyst loading can be tuned. As shown in Figure 1e, a monotonic increase in the average particle size and standard deviation are observed with respect to cycle number, which is consistent with previous reports of other metallic ALD catalysts.⁴⁰ For example, after 510 cycles, the average particle size is 7.8 ± 0.9 nm, which increases to 39.8 ± 8.5 nm after 2040 Cu cycles. Importantly, the conformal nature of PEALD enables this control of the catalyst morphology and loading without clogging the surface pores. An image of an uncoated GDE is included for reference in the Supporting Information (Figure S1), and cross-sectional SEM imaging with elemental mapping are shown in Figure 3, further demonstrating the conformality of the PEALD growth deep within the porous GDE.

To provide a higher resolution visualization of the PEALD Cu catalysts on the GDE surface, scanning transmission electron microscopy (STEM) analysis was performed on a sample after 1020 ALD cycles (Figure 1f). Energy electron loss spectroscopy (EELS) mapping of the Cu and C signals

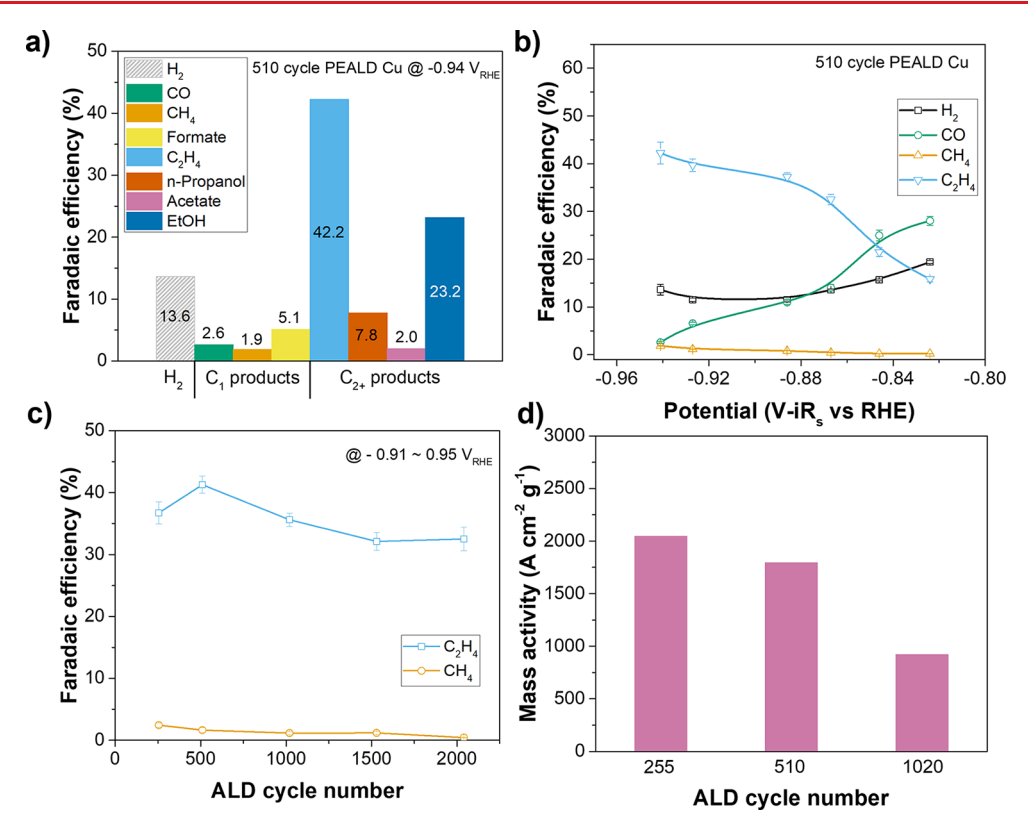


Figure 2. Electrochemical performance of PEALD Cu catalysts. (a) FE of gaseous and liquid products for a 510-cycle PEALD catalyst at -0.94 V vs RHE. (b) FE distribution of gaseous products as a function of the applied potential for a 510-cycle PEALD catalyst. (c) Changes in C_2H_4 and CH_4 FE values according to changes in the ALD cycle number of PEALD catalysts. (d) Comparison of mass activity according to ALD cycle number of PEALD catalysts at -0.91 V to 0.95 V vs RHE. Error bars are based on measurements from three independent samples.

demonstrated that the presence of Cu was localized within these nanoparticle catalyst regions (Figure 1f).

The effect of the ALD cycle number on increased catalyst loading was further illustrated using X-ray photoelectron spectroscopy (XPS) analysis. As shown in Figure 1g, an increase in the ALD cycle numbers results in an increase in the Cu $2p_{3/2}$ and $2p_{1/2}$ signal intensity. The binding energy of these peaks corresponds with the Cu(0)/Cu(I) oxidation state, which is difficult to further deconvolute using XPS. 50 To analyze the crystalline phase of the PEALD films, grazingincidence X-ray diffraction (GIXRD) was performed (Figures S2 and S3). GIXRD was performed on a planar Si substrate to eliminate overlap from graphitic carbon substrate peaks and increase the signal-to-noise ratio, where the crystalline FCC phase of Cu was confirmed. Overall, the ability to conformally modify the porous and tortuous GDE surface with Cu nanoparticles, while maintaining tunable control of particle size and loading, highlights the power of ALD for electrocatalyst applications. 40,5

To study the electrocatalytic performance of the PEALD Cu catalysts on GDE substrates, electrochemical $\rm CO_2RR$ experiments were performed under potentiostatic conditions (-0.94 V vs RHE). An H-cell configuration was used (details in the Supporting Information), which serves as a model system and provides a proof-of-concept platform for future integration into flow-cell architectures. Figure 2a shows the liquid and gaseous product analysis for a PEALD Cu catalyst deposited with 510 cycles. High C–C coupling activity was observed, with a Faradaic efficiency (FE) of 42.2% for $\rm C_2H_4$ and a total FE of 75.2% for the entire range of $\rm C_{2+}$ products detected. The ratio of $\rm C_{2+}/\rm C_1$ products was 7.8:1, which represents a selectivity of

88.7% on the total measured carbonaceous products. These values are among the highest performances reported to date for metallic Cu-based catalysts in a H-cell reactor environment (Table S1). Additionally, the product yields were reproducible, with <3% variance in C_2H_4 FE across different samples (Figure S4). Unlike conventional metallic Cu-based catalysts, which often fail to suppress the production of CH₄ at high overpotentials (Table S1), the 510-cycle PEALD catalyst effectively inhibits both CH₄ production and HER over a range of electrode potentials from -0.82 to -0.94 V vs RHE (Figure 2b).

The high C–C coupling activity and CH_4 suppression of the PEALD catalyst are successfully maintained over a range of ALD cycle numbers from 255 to 2040 (Figure 2c; further details in Figure S5), with the highest performance coming from the 510-cycle condition. As seen by the error bars, the selectivity remains reproducible across multiple samples. This highlights the ability to use the programmable control of ALD to tune the catalyst properties on 3-D surfaces.

In addition to the trends in selectivity, another interesting observation was that as the ALD cycle number decreased, the current densities measured during chronoamperometry remained relatively constant (Figure S5). This indicates that the activity of the electrocatalysts does not appreciably decrease, even when the mass loading was reduced. As shown in the SEM analysis, as the ALD cycle number increases, the average nanoparticle size increases (Figure 1a–e). This indicates that the mass activity (quantified in units of A cm $^{-2}$ g $^{-1}$, based on the projected geometric area of the electrode) increases with a decreasing cycle number. Therefore, to quantitatively measure the mass of Cu deposited over a

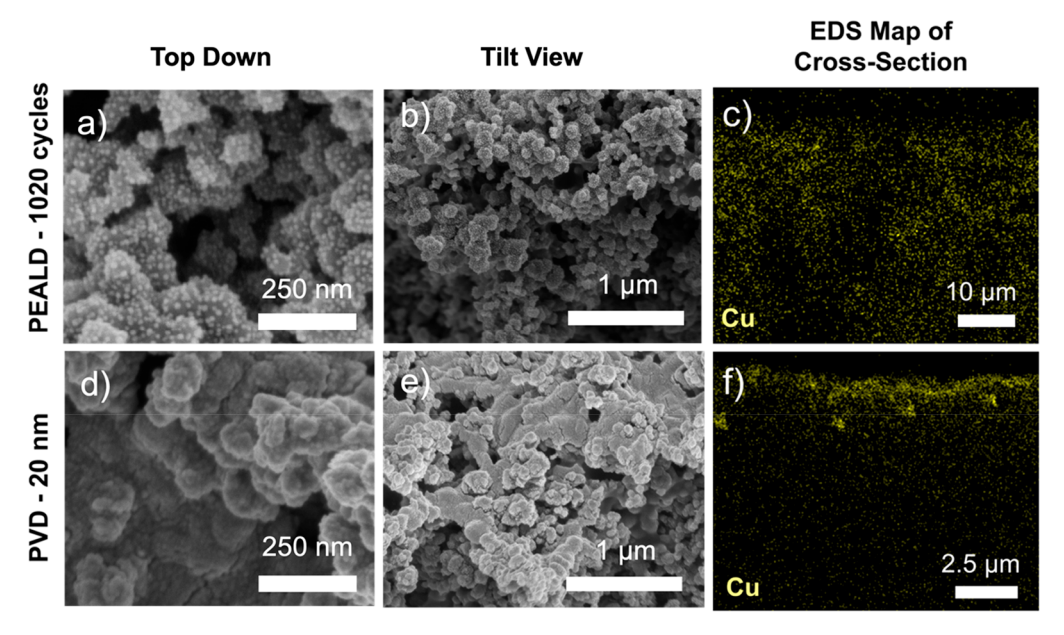


Figure 3. SEM of PEALD Cu with 1020 Cu cycles: (a) top down, (b) tilt view, and (c) cross-sectional EDS Cu map throughout the microporous layer. SEM of 20 nm of the PVD method: (d) top-down, (e) tilt view, and (f) cross-sectional EDS Cu map throughout the microporous layer.

1 cm² projected electrode area (areal mass loading), inductively coupled plasma mass spectrometry (ICP-MS) analysis was performed (Table S2). Consistent with the increase in XPS signal intensity as well as complementary X-ray fluorescence (XRF) analysis (Table S2), the mass loading of Cu increases as the ALD cycle number increases. This allowed for an estimation of the areal mass activity, which is shown in Figure 2d. The calculated mass activity of the PEALD catalyst was found to be 2045.7 A cm⁻² g⁻¹ for 255 ALD cycles, which decreases to 920.1 A cm⁻² g⁻¹ for 1020 cycles. These data demonstrate another powerful benefit of the PEALD process to co-optimize the performance and catalyst mass activity, which has the potential to optimize cost-to-performance ratios when moving to scaled-up manufacturing processes in the future.

In general, it is known that the activity and selectivity of Cubased electrocatalysts for CO₂RR are influenced by a number of factors, including differences in the initial chemical state (e.g., oxidation state), ^{52,53} defect and undercoordinated site density, ^{54–56} catalyst size, shape, and faceting, ^{57–59} local pH gradients along the electrode/electrolyte interface, ^{7,60} and proton transfer limitations based on changes in surface hydrophobicity. ^{16,61} In the future, further detailed studies will be valuable to fully elucidate the origins of the observed trends in selectivity and activity for the PEALD catalyst. However, to provide a baseline comparison with alternative vapor deposition methods, we performed a comparative study with Cu catalysts deposited on the same GDE substrates using thermal evaporation, a common physical vapor deposition (PVD) method.

To compare the activity and selectivity of PEALD vs PVD Cu catalysts, we tested a set of samples where the catalyst mass loading was held approximately constant. Specifically, a PVD deposition with a thickness of 20 nm was compared to a PEALD deposition after 1020 cycles. This corresponded to a similar areal mass loading of the Cu catalyst materials on the GDE substrate, as verified by ICP-MS (Table S2). The PVD Cu sample was confirmed to be phase-pure Cu by GIXRD (Figure S6). Furthermore, XPS analysis on the PVD Cu

illustrated the presence of the Cu(0)/Cu(I) oxidation state, which was consistent with the PEALD Cu samples (Figure S7).

Although the mass loadings of the PEALD and PVD methods are similar, the conformality and catalyst distribution within the porous GDE template were observed to be significantly different. To visualize the differences in catalyst morphology and distribution, top-down and cross-sectional SEM imaging was performed (Figure 3). As shown in Figure 3a-c, the PEALD samples exhibit a discrete nanoparticle morphology, which is conformally maintained deep within the microporous layer of the GDE (additional SEM imaging is provided in Figure S8). As a result, the porosity of the GDE is retained, which is important to maintain the mass transport properties of the GDE and to ensure a high contact area between the electrolyte and catalyst particles throughout the electrode volume.

In contrast, the PVD samples form a denser morphology that is localized near the top surface of the microporous layer of the GDE (Figure 3d-f). As a consequence, the surface porosity of the GDE is significantly decreased because of pore clogging. Furthermore, owing to the line-of-sight nature of PVD, the conformality of the Cu is significantly reduced compared to that of PEALD, resulting in a high concentration of Cu near the top surface of the GDE, with minimal catalyst coverage deeper within the microporous layer. These differences in conformality were confirmed using cross-sectional energy-dispersive X-ray spectroscopy (EDS) mapping (Figure 3c,f). As shown quantitatively in Figure S9, the ALD Cu content was significantly more consistent with respect to depth in comparison to the PVD, where there is a large Cu gradient throughout the first 5 μ m. We further note that the depth of infiltration into porous GDEs is typically not reported in most studies of Cu deposition (Table S3). The present study highlights the importance of this parameter in the design of 3D electrode architectures to deepen our understanding of the factors that control selectivity and activity.

To compare the electrochemical properties of the PEALD and PVD samples, we performed CO₂RR experiments. At a

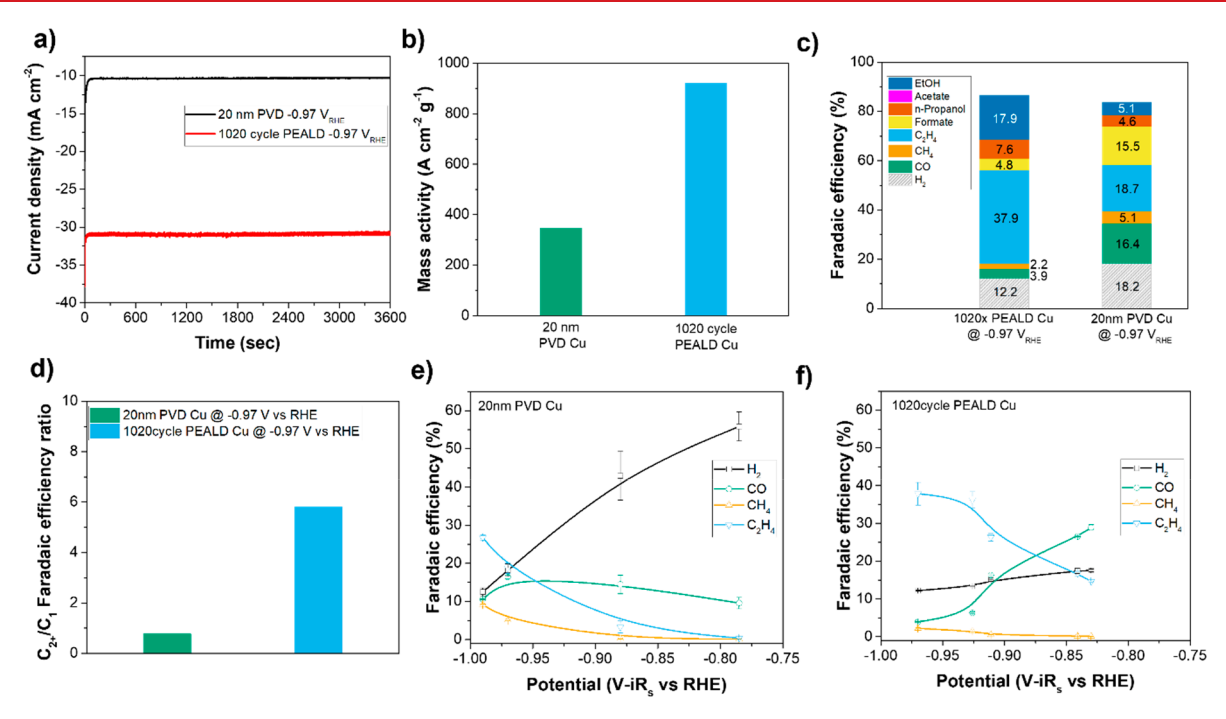


Figure 4. Comparison of FE, product selectivity, and mass activity using a 1020-cycle ALD catalyst vs. a 20 nm PVD catalyst. (a) Current density comparison at -0.97 V vs RHE. (b) Comparison of mass activity difference at -0.97 V vs RHE. (c) FE comparison. (d) Comparison of C₂₊ to C₁ ratio. (e) FE of PVD Cu 20 nm catalyst trend at different potentials. (f) FE of 1020-cycle PEALD Cu catalyst trend at different potentials.

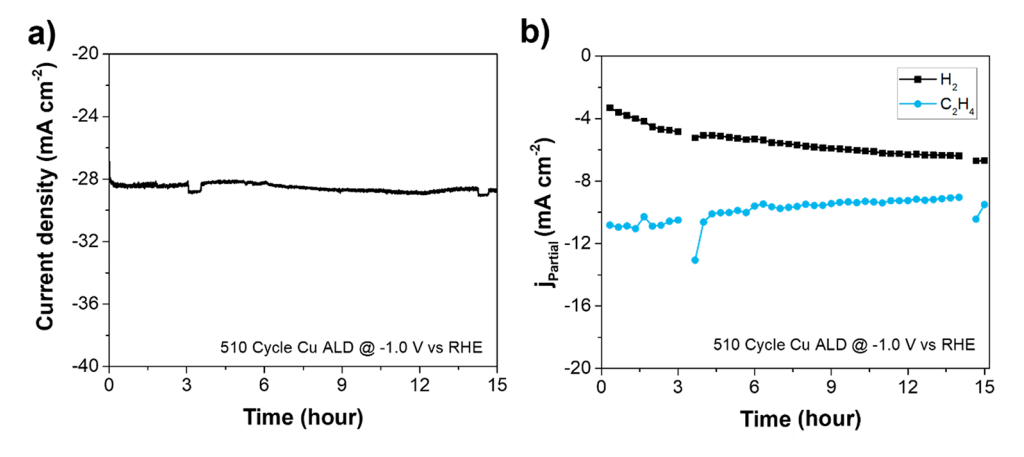


Figure 5. Stability results of 510-cycle PEALD catalysts: (a) C_2H_4 and H_2 partial current densities of the 510-cycle PEALD catalyst at -1.0 V vs RHE for 15 h. (b) Current density of 510-cycle PEALD catalyst for 15 h at -1.0 V vs RHE.

potential of -0.97 V vs RHE, a significant difference was observed between the current densities for the two samples. The PEALD sample exhibited a steady-state current density of 31 mA cm⁻² (mass activity 920.1 A cm⁻² g⁻¹), while the current density for the PVD sample was 10.3 mA cm⁻² (mass activity 345.4 A cm⁻² g⁻¹) (Figure 4a,b). This factor of 3 difference in electrocatalyst activity is attributed to the differences in morphology and catalyst distribution throughout the GDE, as shown in Figure 3. Specifically, the observed differences in the catalyst morphology (surface area, particle size, and infiltration depth) as well as pore clogging will affect the current—overpotential relationship. This highlights the benefits of (PE)ALD to engineer 3-D electrocatalyst architectures, which builds upon prior examples for other reactions. 40,62

There is also a significant difference in product selectivity between the PEALD and PVD samples (Figure 4c,

reproducibility shown in Figure S10). In particular, a higher FE of C-C coupling was observed for the PEALD samples compared to the PVD samples. Specifically, at a potential of -0.97 V vs RHE, the total FE of C_{2+} products was 63.4%, while that of the PVD sample was only 28.4%, representing a >2× difference. Furthermore, the PEALD sample effectively suppresses the generation of CH₄ and CO, with respective FEs of 2.2% and 3.9%, while the FE for CH₄ and CO is significantly higher (5.1% and 16.4%, respectively), indicating a reduced suppression of C_1 products. Overall, the ratio of C_{2+}/C_1 products for the PEALD sample was 5.8:1, while that of the PVD sample was less than 1:1 (Figure 4d). This represents a factor of 7.6× higher selectivity for C-C coupling in the PEALD samples compared to the PVD samples. These trends are observed not only at -0.97 V vs RHE but also over the entire potential range, where the PEALD catalysts effectively suppress hydrogen and CH₄ production (Figure 4e,f). These

Nano Letters pubs.acs.org/NanoLett Letter

trends of reduced activity and selectivity for PVD compared to PEALD were also observed when the thickness of the PVD sample was reduced to 10 nm, which is directly comparable to the 510× PEALD condition (Figure S11).

When considering the possible contributing factors to the observed differences between PEALD and PVD, the most apparent differences relate to the catalyst morphology and distribution. For example, the PEALD catalyst grows as discrete islands, whereas PVD Cu forms a more continuous film morphology. This will influence multiple factors in the electrochemistry of the system, including the presence of surface defects (such as edge sites), differences in surface oxidation, formation of local pH gradients (which will be strongly influenced by the changes in surface porosity and infiltration depth), and bubble formation dynamics. As shown by the XRD and XPS analysis, no obvious differences were observed in the phase and/or chemical state of Cu, although in the future techniques such as X-ray absorption spectroscopy would be beneficial to further elucidate any potential differences in the local coordination environment. However, this study clearly shows the importance of developing and understanding advanced processing methods such as PEALD for 3-D electrocatalyst architectures.

To assess the stability of the PEALD catalyst, the evolution of $\rm CO_2RR$ products was monitored over a period of 15 h for the 510-cycle samples (Figure 5 and Figure S12). As shown in Figure 5a, the total current density (activity) of the catalyst only varied by ~3.5% over the 15 h period. Furthermore, the FE of $\rm C_2H_4$ production remained >30% over the 15 h period, with prolonged suppression of HER (Figure S12). The $\rm C_2H_4$ partial current density also remained relatively stable between $\rm -11$ and $\rm -9~mA~cm^{-2}$ over 15 h. These results demonstrate that PEALD catalysts enable stable $\rm CO_2RR$ even with minimal catalyst loadings, highlighting the potential of ALD for electrolyzer applications in the future.

In this study, Cu catalysts were synthesized via PEALD on GDE substrates and were studied for the $\rm CO_2RR$. By varying the number of ALD cycles, the catalyst size and loading could be tuned at the nanoscale, while maintaining conformal coverage of the 3-D GDE surface. Under optimized conditions, the PEALD catalysts exhibited a FE of 42% for $\rm C_2H_4$ and a total FE of 75.2% for $\rm C_{2+}$ products, which are among the highest values reported to date for Cu catalysts in H-cell geometries. Moreover, the PEALD catalysts demonstrated high methane and hydrogen suppression, reaching $\rm C_2H_4/CH_4$ ratios of 22.2 at -0.9 V vs RHE.

The conformal PEALD coatings enabled uniform infiltration into the GDEs without significantly altering their porosity. In contrast, PVD (evaporated) Cu exhibited a gradient in catalyst loading throughout the GDE thickness and a reduction in surface porosity. As a result of these differences, the mass activity and C_{2+}/C_1 product selectivity for the PVD samples were significantly lower than those for PEALD catalysts. Finally, a stable current density was observed for 15 h using a PEALD catalyst, with minimal changes in the C_2H_4 production rate.

In the future, PEALD can serve as a "toolbox" for the rational design of more complex catalyst materials and architectures to further improve the selectivity and stability. Furthermore, this work provides a pathway toward scalable manufacturing of 3-D electrodes for future integration into industrially relevant electrolyzer formats including flow cells.

ASSOCIATED CONTENT

5 Supporting Information

The Supporting Information is available free of charge at https://pubs.acs.org/doi/10.1021/acs.nanolett.3c02917.

Experimental methods, further experimental details on electrochemical cell and GC setup, additional materials characterization (SEM, XRD), ICP-MS and XRF tables, electrochemical reproducibility tests, table summarizing current copper CO₂RR literature, table and plots of Cu infiltration depth, complete gas products analysis of stability test, methods of *iR* compensation (PDF)

■ AUTHOR INFORMATION

Corresponding Authors

Neil P. Dasgupta — Department of Materials Science and Engineering, University of Michigan, Ann Arbor, Michigan 48109, United States; Department of Mechanical Engineering, University of Michigan, Ann Arbor, Michigan 48109, United States; orcid.org/0000-0002-5180-4063; Email: ndasgupt@umich.edu

Charles A. Roberts — Toyota Research Institute of North America, Ann Arbor, Michigan 48105, United States; orcid.org/0000-0003-4268-8379; Email: charles.roberts@toyota.com

Authors

- Julia D. Lenef Department of Materials Science and Engineering, University of Michigan, Ann Arbor, Michigan 48109, United States
- Si Young Lee Department of Mechanical Engineering, University of Michigan, Ann Arbor, Michigan 48109, United States
- Kalyn M. Fuelling Department of Materials Science and Engineering, University of Michigan, Ann Arbor, Michigan 48109, United States; oorcid.org/0009-0004-1038-4746
- Kevin E. Rivera Cruz Department of Chemistry, University of Michigan, Ann Arbor, Michigan 48109, United States; orcid.org/0000-0001-6690-1571
- Aditya Prajapati Materials Science Division (MSD), Lawrence Livermore National Laboratory, Livermore, California 94550, United States
- Daniel O. Delgado Cornejo Department of Materials Science and Engineering, University of Michigan, Ann Arbor, Michigan 48109, United States; orcid.org/0009-0002-3484-5960
- Tae H. Cho Department of Mechanical Engineering, University of Michigan, Ann Arbor, Michigan 48109, United States
- Kai Sun Department of Materials Science and Engineering, University of Michigan, Ann Arbor, Michigan 48109, United States; orcid.org/0000-0003-1745-9136
- Eugenio Alvarado Department of Chemistry, University of Michigan, Ann Arbor, Michigan 48109, United States
- Timothy S. Arthur Toyota Research Institute of North America, Ann Arbor, Michigan 48105, United States; orcid.org/0000-0003-4348-0756
- Christopher Hahn Materials Science Division (MSD), Lawrence Livermore National Laboratory, Livermore, California 94550, United States; orcid.org/0000-0002-2772-6341
- Charles C. L. McCrory Department of Chemistry and Macromolecular Science and Engineering Program, University

of Michigan, Ann Arbor, Michigan 48109, United States; orcid.org/0000-0001-9039-7192

Complete contact information is available at: https://pubs.acs.org/10.1021/acs.nanolett.3c02917

Author Contributions

J.D.L. and S.Y.L. contributed equally to this work.

Notes

The authors declare no competing financial interest.

ACKNOWLEDGMENTS

This research was supported by Toyota Research Institute of North America (TRINA). This material is based upon work supported by the National Science Foundation under Grant No. 2131709. The authors also thank Dr. Andrew Gayle for assistance with the experimental setups. Work from A.P. and C.H. was performed under the auspices of the U.S. Department of Energy by Lawrence Livermore National Laboratory under Contract DE-AC52-07NA27344 and was supported by Laboratory Directed Research and Development funding under project 22-SI-006 with LLNL release no. LLNL-JRNL- 852808. We thank Dr. Russell E. Bornschein for the performance of ICP-MS measurements. K.E.R.C. acknowledges additional partial support from a Ford Foundation Pre-Doctoral Fellowship and a National GEM Consortium. Portions of this work were performed in the Michigan Center for Materials Characterization and the Lurie Nanofabrication Facility, which are supported by the University of Michigan's College of Engineering.

REFERENCES

- (1) Climate Change: Atmospheric Carbon Dioxide | NOAA Climate.gov. http://www.climate.gov/news-features/understanding-climate/climate-change-atmospheric-carbon-dioxide (accessed 2023-07-27).
- (2) Nitopi, S.; Bertheussen, E.; Scott, S. B.; Liu, X.; Engstfeld, A. K.; Horch, S.; Seger, B.; Stephens, I. E. L.; Chan, K.; Hahn, C.; Nørskov, J. K.; Jaramillo, T. F.; Chorkendorff, I. Progress and Perspectives of Electrochemical CO₂ Reduction on Copper in Aqueous Electrolyte. *Chem. Rev.* **2019**, *119* (12), 7610–7672.
- (3) Qiao, J.; Liu, Y.; Hong, F.; Zhang, J. A Review of Catalysts for the Electroreduction of Carbon Dioxide to Produce Low-Carbon Fuels. *Chem. Soc. Rev.* **2014**, 43 (2), 631–675.
- (4) Kuhl, K. P.; Cave, E. R.; Abram, D. N.; Jaramillo, T. F. New Insights into the Electrochemical Reduction of Carbon Dioxide on Metallic Copper Surfaces. *Energy Environ. Sci.* **2012**, *5* (5), 7050–7059
- (5) Higgins, D.; Hahn, C.; Xiang, C.; Jaramillo, T. F.; Weber, A. Z. Gas-Diffusion Electrodes for Carbon Dioxide Reduction: A New Paradigm. ACS Energy Lett. 2019, 4 (1), 317–324.
- (6) Corral, D.; Feaster, J. T.; Sobhani, S.; DeOtte, J. R.; Lee, D. U.; Wong, A. A.; Hamilton, J.; Beck, V. A.; Sarkar, A.; Hahn, C.; Jaramillo, T. F.; Baker, S. E.; Duoss, E. B. Advanced Manufacturing for Electrosynthesis of Fuels and Chemicals from CO₂. *Energy Environ. Sci.* **2021**, *14* (5), 3064–3074.
- (7) Yang, K. D.; Ko, W. R.; Lee, J. H.; Kim, S. J.; Lee, H.; Lee, M. H.; Nam, K. T. Morphology-Directed Selective Production of Ethylene or Ethane from CO_2 on a Cu Mesopore Electrode. *Angew. Chem.* **2017**, 129 (3), 814–818.
- (8) Hoang, T. T. H.; Verma, S.; Ma, S.; Fister, T. T.; Timoshenko, J.; Frenkel, A. I.; Kenis, P. J. A.; Gewirth, A. A. Nanoporous Copper—Silver Alloys by Additive-Controlled Electrodeposition for the Selective Electroreduction of CO₂ to Ethylene and Ethanol. *J. Am. Chem. Soc.* **2018**, *140* (17), 5791–5797.

- (9) Su, X.; Sun, Y.; Jin, L.; Zhang, L.; Yang, Y.; Kerns, P.; Liu, B.; Li, S.; He, J. Hierarchically Porous Cu/Zn Bimetallic Catalysts for Highly Selective CO₂ Electroreduction to Liquid C₂ Products. *Appl. Catal. B: Environmental* **2020**, 269, No. 118800.
- (10) Kim, C.; Dionigi, F.; Beermann, V.; Wang, X.; Möller, T.; Strasser, P. Alloy Nanocatalysts for the Electrochemical Oxygen Reduction (ORR) and the Direct Electrochemical Carbon Dioxide Reduction Reaction (CO₂RR). *Adv. Mater.* **2019**, *31* (31), No. 1805617.
- (11) Tan, Y. C.; Lee, K. B.; Song, H.; Oh, J. Modulating Local CO_2 Concentration as a General Strategy for Enhancing C–C Coupling in CO_2 Electroreduction. *Joule* **2020**, *4* (5), 1104–1120.
- (12) Jeng, E.; Qi, Z.; Kashi, A. R.; Hunegnaw, S.; Huo, Z.; Miller, J. S.; Bayu Aji, L. B.; Ko, B. H.; Shin, H.; Ma, S.; Kuhl, K. P.; Jiao, F.; Biener, J. Scalable Gas Diffusion Electrode Fabrication for Electrochemical CO₂ Reduction Using Physical Vapor Deposition Methods. ACS Applied Material Interfaces 2022, 14 (6), 7731–7740.
- (13) Yang, Y.; Louisia, S.; Yu, S.; Jin, J.; Roh, I.; Chen, C.; Fonseca Guzman, M. V.; Feijóo, J.; Chen, P.-C.; Wang, H.; Pollock, C. J.; Huang, X.; Shao, Y.-T.; Wang, C.; Muller, D. A.; Abruña, H. D.; Yang, P. Operando Studies Reveal Active Cu Nanograins for CO₂ Electroreduction. *Nature* **2023**, *614* (7947), 262–269.
- (14) Nguyen, T. N.; Dinh, C.-T. Gas Diffusion Electrode Design for Electrochemical Carbon Dioxide Reduction. *Chem. Soc. Rev.* **2020**, *49* (21), 7488–7504.
- (15) Hoang, T. T. H.; Ma, S.; Gold, J. I.; Kenis, P. J. A.; Gewirth, A. A. Nanoporous Copper Films by Additive-Controlled Electrodeposition: CO₂ Reduction Catalysis. *ACS Catal.* **2017**, 7 (5), 3313–3321.
- (16) García de Arquer, F. P.; Dinh, C.-T.; Ozden, A.; Wicks, J.; McCallum, C.; Kirmani, A. R.; Nam, D.-H.; Gabardo, C.; Seifitokaldani, A.; Wang, X.; Li, Y. C.; Li, F.; Edwards, J.; Richter, L. J.; Thorpe, S. J.; Sinton, D.; Sargent, E. H. CO₂ Electrolysis to Multicarbon Products at Activities Greater than 1 A Cm⁻². *Science* **2020**, *367* (6478), 661–666.
- (17) Li, C. W.; Ciston, J.; Kanan, M. W. Electroreduction of Carbon Monoxide to Liquid Fuel on Oxide-Derived Nanocrystalline Copper. *Nature* **2014**, *508* (7497), 504–507.
- (18) Dhakar, S.; Nama, J.; Kumari, V.; Khatua, R.; Mondal, A.; Sharma, S. Ethanol Formation via CO_2 Electroreduction at Low Overvoltage over Exposed (111) Plane of CuO Thin Film. *Electrochim. Acta* **2023**, *441*, No. 141791.
- (19) Cheng, J.; Bai, Y.; Wei, Z.; Mu, Q.; Sun, H.; Lin, L.; Xiao, L.; Xie, X.; Deng, Z.; Peng, Y. Design of Experiments Unravels Insights into Selective Ethylene or Methane Production on Evaporated Cu Catalysts. J. Energy Chem. 2022, 75, 422–429.
- (20) O'Brien, C. P.; Miao, R. K.; Liu, S.; Xu, Y.; Lee, G.; Robb, A.; Huang, J. E.; Xie, K.; Bertens, K.; Gabardo, C. M.; Edwards, J. P.; Dinh, C.-T.; Sargent, E. H.; Sinton, D. Single Pass CO₂ Conversion Exceeding 85% in the Electrosynthesis of Multicarbon Products via Local CO₂ Regeneration. ACS Energy Lett. 2021, 6 (8), 2952–2959.
- (21) Singh, J. A.; Yang, N.; Bent, S. F. Nanoengineering Heterogeneous Catalysts by Atomic Layer Deposition. *Annual Review of Chemical Biomolecular Engineering* **2017**, *8*, 41–62.
- (22) Welch, A. J.; Fenwick, A. Q.; Böhme, A.; Chen, H.-Y.; Sullivan, I.; Li, X.; DuChene, J. S.; Xiang, C.; Atwater, H. A. Operando Local pH Measurement within Gas Diffusion Electrodes Performing Electrochemical Carbon Dioxide Reduction. *J. Phys. Chem. C* **2021**, 125, 20896.
- (23) Bohme, A.; Bui, J. C.; Fenwick, A. Q.; Bhide, R.; Feltenberger, C. N.; Welch, A. J.; King, A. J.; Bell, A. T.; Weber, A. Z.; Ardo, S.; Atwater, H. A. Direct Observation of the Local Microenvironment in Inhomogeneous CO₂ Reduction Gas Diffusion Electrodes via Versatile pOH Imaging. *Energy Environ. Sci.* **2023**, *16* (4), 1783–1795.
- (24) Bok, J.; Lee, S. Y.; Lee, B.-H.; Kim, C.; Nguyen, D. L. T.; Kim, J. W.; Jung, E.; Lee, C. W.; Jung, Y.; Lee, H. S.; Kim, J.; Lee, K.; Ko, W.; Kim, Y. S.; Cho, S.-P.; Yoo, J. S.; Hyeon, T.; Hwang, Y. J. Designing Atomically Dispersed Au on Tensile-Strained Pd for

- Efficient CO₂ Electroreduction to Formate. J. Am. Chem. Soc. 2021, 143 (14), 5386-5395.
- (25) George, S. M. Atomic Layer Deposition: An Overview. *Chem. Rev.* **2010**, *110* (1), 111–131.
- (26) Gayle, A. J.; Berquist, Z. J.; Chen, Y.; Hill, A. J.; Hoffman, J. Y.; Bielinski, A. R.; Lenert, A.; Dasgupta, N. P. Tunable Atomic Layer Deposition into Ultra-High-Aspect-Ratio (>60000:1) Aerogel Monoliths Enabled by Transport Modeling. *Chem. Mater.* **2021**, 33 (14), 5572–5583.
- (27) Johnson, R. W.; Hultqvist, A.; Bent, S. F. A Brief Review of Atomic Layer Deposition: From Fundamentals to Applications. *Mater. Today* **2014**, *17* (5), 236–246.
- (28) Baker, L.; Cavanagh, A. S.; Seghete, D.; George, S. M.; Mackus, A. J. M.; Kessels, W. M. M.; Liu, Z. Y.; Wagner, F. T. Nucleation and Growth of Pt Atomic Layer Deposition on Al2O3 Substrates Using (Methylcyclopentadienyl)-Trimethyl Platinum and O₂ Plasma. *J. Appl. Phys.* **2011**, *109* (8), No. 084333.
- (29) Kim, H. Characteristics and Applications of Plasma Enhanced-Atomic Layer Deposition. *Thin Solid Films* **2011**, *519* (20), 6639–6644.
- (30) Wu, L.; Eisenbraun, E. Effects of Hydrogen Plasma Treatments on the Atomic Layer Deposition of Copper. *Electrochemical Solid-State Letters* **2008**, *11* (5), H107.
- (31) Hagen, D. J.; Connolly, J.; Povey, I. M.; Rushworth, S.; Pemble, M. E. Island Coalescence during Film Growth: An Underestimated Limitation of Cu ALD. *Advanced Materials Interfaces* **2017**, *4* (18), No. 1700274.
- (32) Elam, J. W.; Zinovev, A. V. V.; Pellin, M. J.; Comstock, D. J.; Hersam, M. C. Nucleation and Growth of Noble Metals on Oxide Surfaces Using Atomic Layer Deposition. *ECS Trans.* **2007**, 3 (15), 271.
- (33) Cheng, N.; Stambula, S.; Wang, D.; Banis, M. N.; Liu, J.; Riese, A.; Xiao, B.; Li, R.; Sham, T.-K.; Liu, L.-M.; Botton, G. A.; Sun, X. Platinum Single-Atom and Cluster Catalysis of the Hydrogen Evolution Reaction. *Nat. Commun.* **2016**, *7* (1), No. 13638.
- (34) Yan, H.; Cheng, H.; Yi, H.; Lin, Y.; Yao, T.; Wang, C.; Li, J.; Wei, S.; Lu, J. Single-Atom Pd1/Graphene Catalyst Achieved by Atomic Layer Deposition: Remarkable Performance in Selective Hydrogenation of 1,3-Butadiene. *J. Am. Chem. Soc.* **2015**, *137* (33), 10484–10487.
- (35) Le Formal, F.; Tetreault, N.; Cornuz, M.; Moehl, T.; Gratzel, M.; Sivula, K. Passivating Surface States on Water Splitting Hematite Photoanodes with Alumina Overlayers. *Chemical Science* **2011**, 2 (4), 737–743.
- (36) Lu, J.; Fu, B.; Kung, M. C.; Xiao, G.; Elam, J. W.; Kung, H. H.; Stair, P. C. Coking- and Sintering-Resistant Palladium Catalysts Achieved Through Atomic Layer Deposition. *Science* **2012**, 335 (6073), 1205–1208.
- (37) Chen, Y. W.; Prange, J. D.; Dühnen, S.; Park, Y.; Gunji, M.; Chidsey, C. E. D.; McIntyre, P. C. Atomic Layer-Deposited Tunnel Oxide Stabilizes Silicon Photoanodes for Water Oxidation. *Nat. Mater.* **2011**, *10* (7), 539–544.
- (38) Cao, K.; Cai, J.; Liu, X.; Chen, R. Review Article: Catalysts Design and Synthesis via Selective Atomic Layer Deposition. *Journal of Vacuum Science & Technology A* **2018**, 36 (1), No. 010801.
- (39) O'Neill, B. J.; Jackson, D. H. K.; Lee, J.; Canlas, C.; Stair, P. C.; Marshall, C. L.; Elam, J. W.; Kuech, T. F.; Dumesic, J. A.; Huber, G. W. Catalyst Design with Atomic Layer Deposition. *ACS Catal.* **2015**, 5 (3), 1804–1825.
- (40) Dasgupta, N. P.; Liu, C.; Andrews, S.; Prinz, F. B.; Yang, P. Atomic Layer Deposition of Platinum Catalysts on Nanowire Surfaces for Photoelectrochemical Water Reduction. *J. Am. Chem. Soc.* **2013**, 135 (35), 12932–12935.
- (41) Pickrahn, K. L.; Park, S. W.; Gorlin, Y.; Lee, H.-B.-R.; Jaramillo, T. F.; Bent, S. F. Active MnOx Electrocatalysts Prepared by Atomic Layer Deposition for Oxygen Evolution and Oxygen Reduction Reactions. *Adv. Energy Mater.* **2012**, *2* (10), 1269–1277.
- (42) Hu, S.; Shaner, M. R.; Beardslee, J. A.; Lichterman, M.; Brunschwig, B. S.; Lewis, N. S. Amorphous TiO2 Coatings Stabilize

- Si, GaAs, and GaP Photoanodes for Efficient Water Oxidation. *Science* **2014**, 344 (6187), 1005–1009.
- (43) Jiang, X.; Gür, T. M.; Prinz, F. B.; Bent, S. F. Atomic Layer Deposition (ALD) Co-Deposited Pt—Ru Binary and Pt Skin Catalysts for Concentrated Methanol Oxidation. *Chem. Mater.* **2010**, 22 (10), 3024—3032.
- (44) Ren, D.; Gao, J.; Pan, L.; Wang, Z.; Luo, J.; Zakeeruddin, S. M.; Hagfeldt, A.; Grätzel, M. Atomic Layer Deposition of ZnO on CuO Enables Selective and Efficient Electroreduction of Carbon Dioxide to Liquid Fuels. *Angew. Chem., Int. Ed.* **2019**, *58* (42), 15036–15040.
- (45) Schreier, M.; Héroguel, F.; Steier, L.; Ahmad, S.; Luterbacher, J. S.; Mayer, M. T.; Luo, J.; Grätzel, M. Solar Conversion of CO₂ to CO Using Earth-Abundant Electrocatalysts Prepared by Atomic Layer Modification of CuO. *Nature Energy* **2017**, 2 (7), 1–9.
- (46) Suominen, M.; Mäntymäki, M.; Mattinen, M.; Sainio, J.; Putkonen, M.; Kallio, T. Electrochemical Reduction of CO₂ to Formate in a Flow Cell on CuSx Grown by Atomic Layer Deposition. *Materials Today Sustainability* **2023**, 24, No. 100575.
- (47) Gao, F.; Jiang, J.; Du, L.; Liu, X.; Ding, Y. Stable and Highly Efficient Cu/TiO₂ Nanocomposite Photocatalyst Prepared through Atomic Layer Deposition. *Appl. Catal. A: General* **2018**, *568*, 168–175.
- (48) Liu, M.; Zheng, L.; Bao, X.; Wang, Z.; Wang, P.; Liu, Y.; Cheng, H.; Dai, Y.; Huang, B.; Zheng, Z. Substrate-Dependent ALD of Cux on TiO₂ and Its Performance in Photocatalytic CO₂ Reduction. *Chem. Eng. J.* **2021**, 405, No. 126654.
- (49) Guo, Z.; Li, H.; Chen, Q.; Sang, L.; Yang, L.; Liu, Z.; Wang, X. Low-Temperature Atomic Layer Deposition of High Purity, Smooth, Low Resistivity Copper Films by Using Amidinate Precursor and Hydrogen Plasma. *Chem. Mater.* **2015**, 27 (17), 5988–5996.
- (50) Biesinger, M. C. Advanced Analysis of Copper X-Ray Photoelectron Spectra: Advanced Analysis of Copper X-Ray Photoelectron Spectra. Surf. Interface Anal. 2017, 49 (13), 1325–1334.
- (51) Lu, J.; Stair, P. C. Low-Temperature ABC-Type Atomic Layer Deposition: Synthesis of Highly Uniform Ultrafine Supported Metal Nanoparticles. *Angew. Chem., Int. Ed.* **2010**, 49 (14), 2547–2551.
- (52) Lee, S. Y.; Jung, H.; Kim, N.-K.; Oh, H.-S.; Min, B. K.; Hwang, Y. J. Mixed Copper States in Anodized Cu Electrocatalyst for Stable and Selective Ethylene Production from CO₂ Reduction. *J. Am. Chem. Soc.* **2018**, *140* (28), 8681–8689.
- (53) Mistry, H.; Varela, A. S.; Bonifacio, C. S.; Zegkinoglou, I.; Sinev, I.; Choi, Y.-W.; Kisslinger, K.; Stach, E. A.; Yang, J. C.; Strasser, P.; Cuenya, B. R. Highly Selective Plasma-Activated Copper Catalysts for Carbon Dioxide Reduction to Ethylene. *Nat. Commun.* **2016**, *7* (1), No. 12123.
- (54) Lee, S. Y.; Chae, S. Y.; Jung, H.; Lee, C. W.; Nguyen, D. L. T.; Oh, H.-S.; Min, B. K.; Hwang, Y. J. Controlling the C2+ Product Selectivity of Electrochemical CO₂ Reduction on an Electrosprayed Cu Catalyst. *Journal of Material Chemistry A* **2020**, 8 (13), 6210–6218.
- (55) Jung, H.; Lee, S. Y.; Lee, C. W.; Cho, M. K.; Won, D. H.; Kim, C.; Oh, H.-S.; Min, B. K.; Hwang, Y. J. Electrochemical Fragmentation of Cu_2O Nanoparticles Enhancing Selective C–C Coupling from CO_2 Reduction Reaction. J. Am. Chem. Soc. 2019, 141 (11), 4624–4633.
- (56) Jeon, H. S.; Kunze, S.; Scholten, F.; Roldan Cuenya, B. Prism-Shaped Cu Nanocatalysts for Electrochemical CO₂ Reduction to Ethylene. *ACS Catal.* **2018**, 8 (1), 531–535.
- (57) De Gregorio, G. L.; Burdyny, T.; Loiudice, A.; Iyengar, P.; Smith, W. A.; Buonsanti, R. Facet-Dependent Selectivity of Cu Catalysts in Electrochemical CO₂ Reduction at Commercially Viable Current Densities. ACS Catal. 2020, 10 (9), 4854–4862.
- (58) Loiudice, A.; Lobaccaro, P.; Kamali, E. A.; Thao, T.; Huang, B. H.; Ager, J. W.; Buonsanti, R. Tailoring Copper Nanocrystals towards C₂ Products in Electrochemical CO₂ Reduction. *Angew. Chem., Int. Ed.* **2016**, *55* (19), 5789–5792.
- (59) Jun, M.; Kwak, C.; Lee, S. Y.; Joo, J.; Kim, J. M.; Im, D. J.; Cho, M. K.; Baik, H.; Hwang, Y. J.; Kim, H.; Lee, K. Microfluidics-Assisted

- Synthesis of Hierarchical Cu₂O Nanocrystal as C₂-Selective CO₂ Reduction Electrocatalyst. *Small Methods* **2022**, *6* (5), No. 2200074. (60) Lu, X.; Zhu, C.; Wu, Z.; Xuan, J.; Francisco, J. S.; Wang, H. In Situ Observation of the pH Gradient near the Gas Diffusion Electrode of CO $_2$ Reduction in Alkaline Electrolyte. *J. Am. Chem. Soc.* **2020**, 142 (36), 15438–15444.
- (61) Wakerley, D.; Lamaison, S.; Ozanam, F.; Menguy, N.; Mercier, D.; Marcus, P.; Fontecave, M.; Mougel, V. Bio-Inspired Hydrophobicity Promotes CO₂ Reduction on a Cu Surface. *Nat. Mater.* **2019**, *18* (11), 1222–1227.
- (62) Patil, B.; Satilmis, B.; Khalily, M. A.; Uyar, T. Atomic Layer Deposition of NiOOH/Ni(OH) $_2$ on PIM-1-Based N-Doped Carbon Nanofibers for Electrochemical Water Splitting in Alkaline Medium. ChemSusChem 2019, 12 (7), 1469–1477.